Excited-State Proton Transfer in Methanol-Doped Ice in the Presence of KF

Anna Uritski and Dan Huppert*

Raymond and Beverly Sackler Faculty of Exact Sciences, School of Chemistry, Tel Aviv University, Tel Aviv 69978, Israel

Received: November 20, 2007; Revised Manuscript Received: February 12, 2008

Steady-state and time-resolved emission techniques were employed to study the photoprotolytic cycle of an excited photoacid in ice in the presence of a low concentration of a weak base-like F^-. In previous studies we found that the photoprotolytic cycle in methanol-doped ice (1% mol fraction) is too slow to be observed at temperatures below 190 K. In this study we found that at temperatures below 240 K an additional proton-transfer process occurs in ice doped with 10 mM KF. We attributed this reaction to the creation of a mobile L-defect by F^- ions. We used a diffusion-assisted reaction model, based on the Debye−Smoluchowski equation, to account for the direct reaction of the L-defect with the excited photoacid at temperatures below $T < 240$ K. Below 160 K the spectroscopic properties as well as the photoprotolytic cycle change dramatically. We propose that below 160 K the sample enters a new phase. The excited-state proton-transfer (ESPT) process was observed and followed down to a liquid nitrogen temperature of ∼78 K. In the low-temperature phase the ESPT rate is almost twice as much as at 180 K and the temperature dependence of the rate is very small. The kinetic isotope effect of the ESPT at the low-temperature phase is small of about 1.3.

Introduction

The physics of ice has been studied extensively for many centuries. The properties of ice were summarized in several books.[1–4] Approximately at the freezing point, the conductance[5] in ice is relatively large; however, it drops rapidly as the temperature decreases. The theory of Jaccard[6] is used to explain the electrical conduction in ice, according to which, the electrical properties of ice are largely due to two types of defects within the crystal structure. Ion defects are produced when a proton moves from one end of the bond to the other, thus creating a H_3O^+, OH^- ion pair. Conduction is then possible by means of successive proton jumps. Bjerrum defects[7] are orientational defects caused by the rotation of a water molecule to produce either a doubly occupied bond (D-defect) or a bond with no protons (L-defect). The mechanism of excess proton transfer in ice was investigated by Ohmine and coworkers[8] using the QM/MM method. By analyzing the potential surface, the normal modes and the interaction between the excess proton and the defects, they proposed that the excess proton is localized in a L-defect in ice. Podeszwa and Buch[9] studied the structure and dynamics of orientational defects in ice by molecular dynamics simulations. They found the defect structure to be quite different from the one originally proposed by Bjerrum.[7] Two basic structures were identified for the D-defect and one dominant structure was obtained for the L-defect. Typically, one water molecule in an L-defect is displaced at ≈1 Å from the crystal lattice site. Defect jumps occur via vibrational phase coincidence.

The proton-transfer reaction in the liquid state was studied extensively.[10–12] Excited-state proton transfer (ESPT) from a photoacid is used as a common tool to study various aspects of proton-transfer reactions, as well as proton conductivity of various protic liquids.[13–20]

In previous studies we used photoacids to inject a proton into ice.[21–23] The phoroprotolytic cycle of a photoacid in liquid and in ice includes two steps, a reactive step followed by a diffusive step.[17] In the reactive step a proton is transferred from a photoacid to a solvent molecule. The proton then diffuses in the liquid solvent or in ice. The deprotonated photoacid geminately recombines with the diffusing proton and repopulates the protonated form of the photoacid. The photoprotolytic cycle can be easily monitored by time-resolved emission techniques. The diffusing proton monitors the microscopic environment surrounding the excited photoacid molecule. The time window of the experiment is limited to about two excited-state lifetimes, i.e., about 10–15 ns. For a proton diffusion constant of about 10^{-4} cm^2/s, the proton provides pertinent information on the microscopic structure within a radius of $r > 100$ Å.

In a more recent study[24] of 2-naphthol-6,8-disulfonate and coumarin 343, we found that the dynamic solvation shift (occurring on the excited-state potential surface) suddenly decreased. This may explain the previous experimental finding that the ESPT process is inefficient below 160 K. We proposed[23] that below 160 K the excited-state proton transfer was inefficient due the solvation energy drop and, as a consequence, the rate suddenly decreased.

In previous study[25] we measured the scavenging dynamics of the ejected proton by a small amount of acetate or fluoride ions only in the high-temperature range of $270 > T > 240$ K. We found that the proton scavenging process was more efficient in ice than in the liquid state, in spite of the fact that the photoacid and the base were immobile in ice. In the present study we extended the temperature range of the previous study down to a liquid nitrogen temperature at about ∼78 K. In the presence of a small concentration of F^- ions (10 mM), in addition to the proton scavenging process, we found that below 240 K another process also takes place. The overall rate of proton transfer increased appreciably in the presence of F^- ions. As mentioned above, the ESPT process is inefficient at temperatures below 180 K and the steady-state emission spectrum below 180 K consists only of the ROH band. The study of solvation dynamics indicates that below 170 K the

* Corresponding author. E-mail: huppert@tulip.tau.ac.il. Phone: 972-6407012. Fax: 972-3-6407491.

10.1021/jp711030m CCC: $40.75
Published on Web 04/22/2008

SCHEME 1

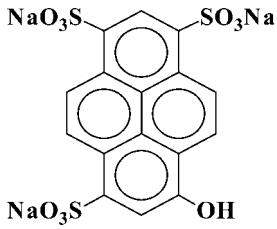

solvation properties do not support a direct proton transfer as observed in liquid and in high-temperature ice down to about 190 K. In the presence of 10 mM KF the ESPT exhibits efficiency at temperatures below 180 K. We found that the effective proton-transfer rate constant at liquid nitrogen temperatures is about 3×10^8 s^{-1} It is slightly larger than the excited-state radiative rate of 2×10^8 s^{-1}.We propose that at temperatures below 240 K, a direct proton transfer occurs from the excited photoacid to a mobile L-defect created by a fluoride. The fluoride ion creates a mobile L-defect capable of reacting with an excited photoacid. L-defect mobility exhibits a low activation energy[26] and can thus approach the excited photoacid, even at very low temperatures.

Experimental Section

We used the time-correlated single-photon counting (TCSPC) technique, to measure the time-resolved emission of the photoacids. For sample excitation, we used a cavity dumped Ti: sapphire femtosecond laser, Mira, Coherent, which provides short, 80 fs, pulses of variable repetition rates, It operates at the SHG frequency over the spectral range of 380–400 nm and at the THG (third harmonic generation) frequency over a spectral range of 260–290 nm with the relatively low repetition rate of 500 kHz. The TCSPC detection system is based on a Hamamatsu 3809U, photomultiplier and Edinburgh Instruments TCC 900 computer module. The overall instrumental response was about 35 ps (FWHM). The excitation pulse energy was reduced by neutral density filters to about 10 pJ.

Steady-state fluorescence spectra at room temperature were taken using a FluoroMax (Jobin Yvon) spectrofluorometer, whereas at a lower temperature we used a miniature CCD spectrograph CVI MS-240. The 8-hydroxy-1,3,6-pyrenetrisulfonate (HPTS, Scheme 1), laser grade was purchased from Kodak. Potassium fluoride was purchased from Fluka. Perchloric acid, 70% reagent grade, was purchased from Aldrich. For steady-state fluorescence measurements we used photoacid solutions of $\sim 2 \times 10^{-5}$ M. For transient measurements the sample concentrations were between 2×10^{-4} and 2×10^{-5}M. Deionized water had a resistance >10 MΩ. Methanol, of analytical grade, was from Fluka. All chemicals were used without further purification. The pH solution was about 6.

The temperature of the irradiated sample was controlled by placing the sample in a liquid N_2 cryostat with a thermal stability of approximately ±1.5 K.

Ice samples were prepared by first placing the cryogenic sample cell for about 20 min at a temperature of about 273 K. The second step involved relatively rapid cooling (10 min) to about 250 K. The sample subsequently froze within 5 min. To ensure ice equilibration prior to time-resolved measurements, the sample temperature was kept for another 30 min at about 250 K.

Reversible Diffusion-Influenced Two-Step Proton-Transfer Model with Inclusion of a Proton Scavenger in Solution. In this model[20,27] the photoprotolytic cycle in the excited state is subdivided into two consecutive steps of reaction and diffusion. The mathematical and computational details are given elsewhere.[26] It is based on solving of the Debye Smoluchowski equation (DSE), coupled to an ordinary chemical kinetic equation. The emitted proton, while diffusing in liquid solution or in ice, may react with a mild base like the acetate or fluoride anion. The reaction is easily observed as a strong reduction of the intensity of the ROH long time fluorescence tail.

To account for the proton reaction with the base anion, we introduced a special bimolecular reaction term.[25] The negatively charged F^- is not evenly distributed around the negatively charged HPTS photoacid molecule in the ground electronic state. As a consequence we used the Debye−Hückel screened Coulomb potential[21] to account for the presence of KF in ice.

Characterization of the Polycrystalline Ice Samples. Pure ice is known to be a bad solvent.[4] It occurs that upon controlled slow freezing most of the dopants are extracted out of the crystal and therefore concentrates at the grain boundary. In our initial experiments on the photoprotolytic cycle of the photoacid in pure ice,[21,22] we noticed that the frozen samples are nonfluorescent, whereas for the liquid samples the fluorescence is at least 3 orders of magnitude more intense. We explained the lack of fluorescence of the photoacid in "pure" ice samples by the aggregation of the photoacid molecules at the grain boundary. Dimerization of two photoacid molecules causes the annihilation of the overall transition dipole moment which will lead to the reduction of the fluorescence intensity. We found a procedure to overcome the aggregation of the photoacid molecules upon sample freezing. To prevent the aggregation, we added to a pure aqueous solution 1% of methanol (by mole ratio). The methanol probably serves as a mediator between the hydrophobic aromatic rings of the photoacid with the ice water molecules. In numerous experiments we found that the fluorescence intensity of the frozen methanol-doped ice sample containing the photoacid is "behaving properly.

Here we list a set of spectroscopic parameters of several photoacids in methanol-doped ice that indicate that the photoacid molecules are indeed in the bulk of the polycrystalline sample and not at the grain boundaries:

1. The time integrated fluorescence intensities (the steady-state spectra) of both ROH and RO^- bands of the photoacid are about the same as for the liquid-state samples. 2. The spectroscopic structures of the steady-state emission of the ROH and RO^- bands in ice are similar to those for the liquid state except for (as expected) a small blue shift and a smaller band width (these parameters are temperature dependent). When both the methanol and the photoacid are excluded while water is frozen, the methanol provides a uniform solvation surface region and the spectroscopic data of the photoacid are expected to be more like those of a photoacid in bulk methanol, rather than those of water. In a methanol solution the proton-transfer rate is slower in pure water by a factor of about 1000. The width and position of the ROH and RO^- bands strongly depend on the solvent. In methanol the RO^- band is blue shifted by about 500 cm^{-1} and the width decreases by about 300 cm^{-1}. This is clearly not the case based on the spectroscopic properties of a photoacid in frozen methanol-doped ice samples. 3. The repeatability and the reproducibility of the steady-state emission spectra as a function of temperature are excellent, as was measured by us for several hundred samples. 4. Time-resolved emission measured by the time correlated single photon counting technique of photoacids in methanol-doped ice at a large temperature range is exactly reproducible with all the fine details of the complex decay pattern along many orders of magnitude.

X-ray diffraction of a methanol-doped frozen water samples (100–270 K) shows a polycrystalline diffraction pattern. The ice structure surrounding the photoacid is far from ideal I_h ice. The relatively large photoacid causes a large mismatch between the structure of the close by shells of methanol-doped water and the actual I_h crystalline structure at a further distance from the photoacid. We suggest that the solvent next to the photoacid is organized in a vitrous ice (amorphous ice) structure rather than crystalline I_h structure. If such an assumption holds, than the proton diffusion in the amorphous region is more likely to have a value similar to that of a super-cooled liquid, rather than that of pure I_h ice.

In a recent paper[28] we characterized the position of the photoacid in methanol-doped ice samples by employing the Förster electronic energy-transfer (FRET) process between two chromophores. We used the FRET process to estimate the average distance between two large aromatic compounds in polycrystalline samples. For a 10 μM cubic crystal and a concentration of 1 mM the average distance between adjacent photoacid molecules at the grain boundaries of a microcrystal of 10 μM size should be equivalent to about 5 Å. We used 8-hydroxy-1,3,6-pyrenetrisulfonate (a commonly used photoacid) in its deprotonated form, RO^- as the FRET donor, and Rhodamine 110 as the acceptor. We compared the time-resolved emission FRET experimental results of samples in aqueous liquid state with the results in ice. The FRET process at concentration of $0.2 < c < 1$ mM of acceptor showed a small and similar energy-transfer rate for both liquid and ice samples (the critical radius, $R_0 = 56$ Å). We concluded that both the donor (the photoacid) and the acceptor at these low concentrations are situated in the bulk of the ice microcrystal rather than at the grain boundaries of the microcrystal, where the distances between donor and acceptor should be much shorter than R_0, and hence the FRET process should be very efficient. The Förster EET experiment indicate that in methanol-doped ice the photoacid molecules tend to stay in the bulk of the microcrystal rather than to aggregate at the grain boundaries upon freezing of the sample.

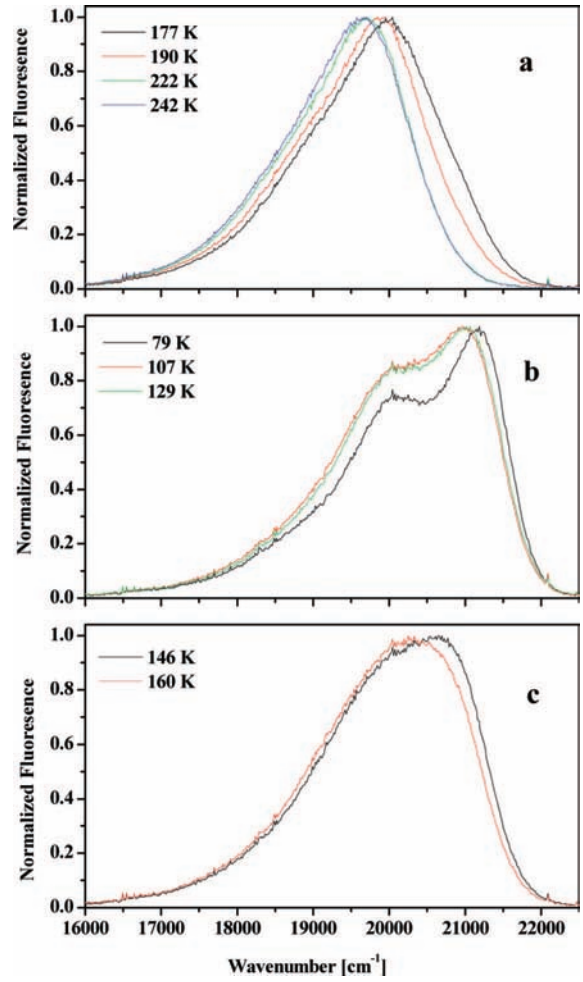

Figure 1. Steady-state emission spectra of HPTS in basic solution in methanol-doped ice (1% mole fraction) at various temperatures: (a) spectra in the high-temperature region of 270 K > T > 175 K; (b) spectra in the low-temperature region of 145 > T > 80 K; (c) spectra in the intermediate temperature range region of 175 K > T > 145 K.

Results

Steady-State Emission. Figure 1 shows the steady-state emission spectra of a basic solution (pH ~ 8.5) of HPTS in methanol-doped ice at various temperatures. Figure 1a shows the spectra in the high-temperature region of 270 > T > 177 K. The RO^- band in this region is broad and structureless. As the temperature lowers the RO^- emission band shifts to the blue and the band width decreases somewhat.

Figure 1b shows the steady-state emission of the RO^- band at several temperatures in the low-temperature region of 140 > T > 75 K. The RO^- emission band consists of several distinguished vibronic bands. We fit the structured emission spectrum by assigning a log-normal line shape function to each vibration band.[29] This type of spectrum is a result of the Franck−Condon principle. When the ground and first electronically excited potential surfaces are displaced, with respect to a generalized coordinate, the relative amplitude of the vibration progression is given by the Huang Rhys factor S_0. The relative amplitude of each individual vibronic peak is given by $S_0^n/n!$, where n is an integer assigned to the specific vibration level in the spectrum. In the low-temperature range the peak position of the RO^- band shifts abruptly to the blue. Below 135 K this occurs at about 475 nm, whereas at 175 K the peak position occurs at ~500 nm.

The parameters for the fit of each vibronic band are the peak position ν_p, the relative height h, the bandwidth $\Delta\nu$ and the asymmetry γ.

In the relatively narrow temperature range below 175 K and above 145 K (the intermediate temperature range) a large change in the RO^- emission is observed. Figure 1c shows the emission spectra of the RO^- band in this range at two temperatures. In the intermediate temperature range the emission spectrum consists of a superposition of two RO^- emission bands, that of the high-temperature phase and that of the low-temperature phase. The band analysis clearly shows that in this region there is a phase transition. At the low-temperature phase, $T < 150$ K, the RO^- emission band shifts strongly to the blue by about 800 cm^{-1} with respect to its position in the high-temperature phase at $T = 185$ K. The bandwidth strongly decreases by about 400 cm^{-1} between the high-temperature phase (T > 177 K) and the low-temperature phase (T < 145 K).

Figure 2 shows a fit of the steady-state experimental data shown in Figure 1 using the approach that a phase transition takes place around 165 K and that the emission spectrum at temperatures close to the phase transition (the intermediate temperature range) consists of two different emission spectra of the RO^- form and the photoacid. The fit of the high-temperature region, (structureless band shape), is easily achieved

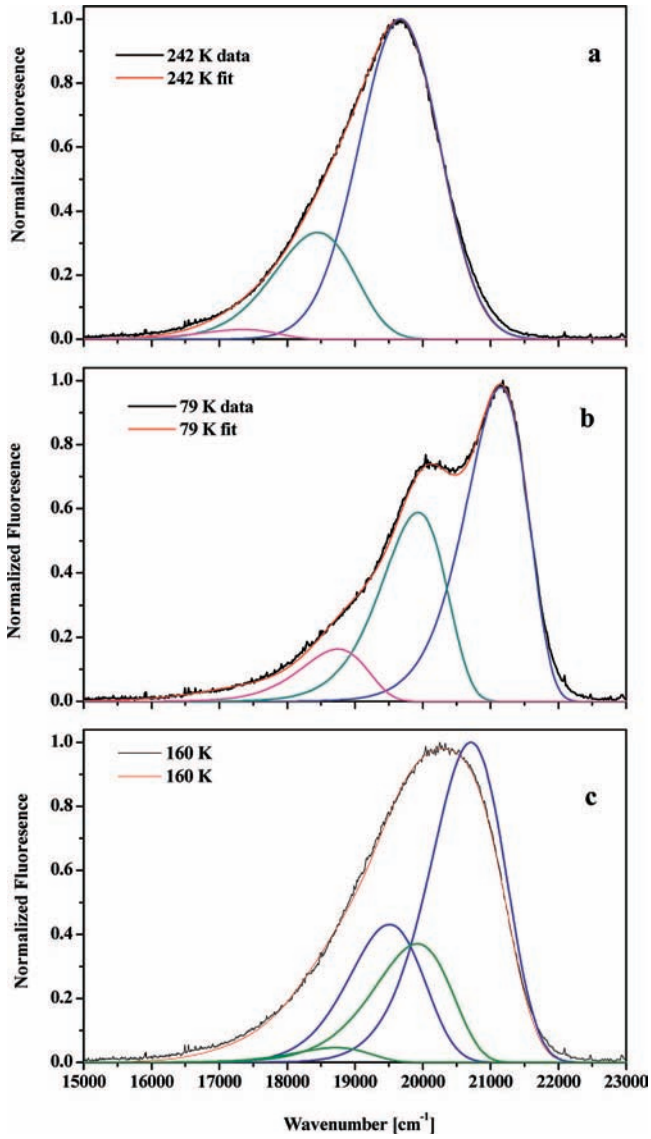

Figure 2. Steady-state emission spectra of the HPTS basic solution (black) and the computer fit (red) using a lognormal function for each vibronic band. The vibronic sub-band is also shown in the figure.

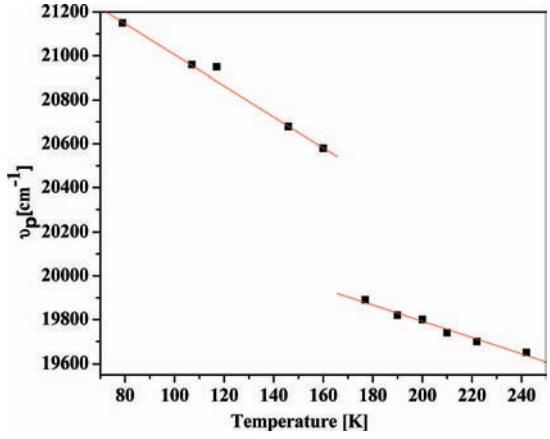

Figure 3. The RO^- peak position of the emission band of HPTS in ice doped with methanol as a function of temperature.

by assigning a larger bandwidth to the individual vibronic bands. As seen in the figure, the fit is rather good at high, intermediate and low-temperatures range.

Figure 3 shows a plot of the RO^- emission band peak position ν_p as a function of temperature. The plot of Figure 3 clearly

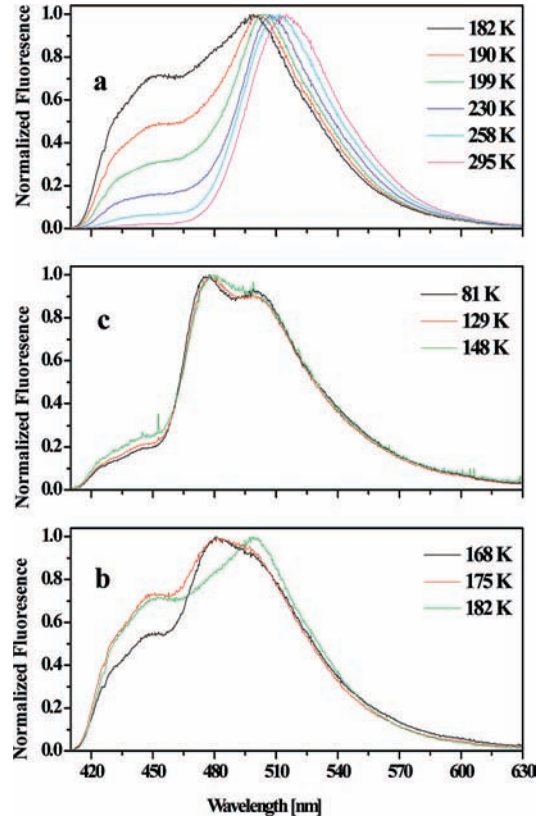

Figure 4. Steady-state emission spectra of HPTS in the presence of 10 mM KF, in slightly acidic methanol-doped ice, at various temperatures: (a) spectra in the high-temperature region; (b) spectra in the low-temperature range 148 K > T > 80 K; (c) spectra in the intermediate temperature range region 180 > T > 160 K.

shows that the RO^- emission band undergoes large changes at its peak position. We also noticed bandwidth narrowing at a relatively narrow and central temperature range of about 175 K.

Figure 4 shows the steady-state emission at several temperatures of a slightly acidic H_2O solution (pH ~ 6) of HPTS in the presence of 10 mM KF. The high-temperature region, 295 K > T > 185 K, is shown in Figure 4a. The spectrum consists of both ROH and RO^- bands. A simple relation connects the relative fluorescence intensities of the two bands with the excited-state proton-transfer rate and the radiative rate

$$\varphi'/\varphi \cong \frac{k_{PT}}{k_{rad}} \tag{1}$$

where φ and φ' are the fluorescence quantum yields of the protonated and deprotonated forms of for the photoacid respectively. k_{PT} and k_{rad} are the rate constants for proton transfer and the radiative process respectively. As the temperature decreases, the proton-transfer rate decreases and the ROH band intensity increases while the RO^- band intensity decreases. At about 200 K the proton-transfer rate constant k_{PT} is much smaller than the radiative rate constant k_{rad}. The emission spectrum consists mainly of a single ROH band.

Figure 4b shows the steady-state emission of a slightly acidic HPTS water-solution containing 10 mM KF in the low-temperature range of T < 160 K. Figure 4c shows the steady-state emission of a slightly acidic HPTS water-solution containing 10 mM KF in the intermediate temperature range of 180 K > T > 160 K. The lower temperature limit of the intermediate range in which the two RO^- bands coexist is shifted

up by about 10 deg from 150 to 160 K when KF is present in the ice sample. As seen in the figure in the intermediate range the spectrum consists of both the ROH band and the two RO^- bands, the band at ~475 nm and at 500 nm band.

The ratio between the fluorescence intensities of the RO^- and ROH bands, I_f^{RO-}/I_f^{ROH}, depends somewhat on the cooling rate of the sample. It decreases upon annealing of the sample (sample warming followed by a sample cooling cycle). As mentioned above, the RO^- emission band intensity in the absence of KF is already negligible at about 200 K. In the presence of 10 mM KF, after the phase transition to the "cold phase", the RO^- emission band appears again in the spectrum (blue shifted by about 800 cm^{-1}). At about 185 K (the upper temperature of the phase transition region) the RO^- band has a complex structure arising from the coexistence of two different emission bands for the RO^-. Similar results were observed in Figure 1c showing the steady-state emission spectrum of a basic sample of HPTS water in the absence of 10 mM KF where the ground-state RO^- form is excited and not the ROH form, as in the case of the acidic solution.

To obtain a good fit to the ROH emission band, we used four lognormal functions for the vibration bands. The two high-energy bands are of about equal intensity, and the relative amplitude of the subsequent two lower energy bands is smaller and has a decreasing amplitude with decreasing emission energy. When $S_0 \approx 1$ (a relatively large displacement between the minima of the ground and electronic states), the intensity of the second vibration band is of about the same intensity as the first one and the intensity of the subsequent vibration bands decreases monotonically. From the band analysis of the emission spectrum of the ROH band at a low temperature the relative intensities of the four vibrations approximately fit the case of $S_0 = 1$. As the temperature decreases, the vibronic peak position and the relative intensities are almost unchanged but their width decreases.

Time-Resolved Emission. Figure 5 shows the time-resolved emission of ROH, the protonated form of HPTS, of two samples at various temperatures in the high-temperature region of 185 K $\leq T \leq$ 270 K. The first sample contains HPTS in ice doped with 1% (mole fraction) methanol, and the second sample also contains 10 mM KF. The samples were excited by 400 nm 150 fs pulses (SHG of a mode locked cavity dumped Ti:sapphire laser) at a repetition rate of 500 kHz. The time-resolved emission was acquired by a time correlated single photon counting technique with an instrumental response function with a full width half maximum of about 35 ps. As seen in the figure, for a particular temperature the fluorescence decay curve of the sample containing 10 mM KF differs from the sample without it. The long time non-exponential tail is strongly reduced in samples containing 10 mM KF. We explain this phenomenon by the efficient reaction of the mobile proton in ice with the static F^- surrounding the excited photoacid molecule. The average distance of an F^- ion from an excited photoacid (very small concentration) is about half the average distance between the F^- ions, which is 55 Å for a 10 mM solution. Thus the proton scavenging reaction takes place at an average distance of about 10 water molecules (the O−O distance in hexagonal ice is ~2.75 Å) from the photoacid itself. The time-resolved data can be fitted by the reversible-geminate recombination model with the inclusion of a proton scavenger in solution.[25]

In addition to the reduced long-time fluorescence tail, one can easily observe that at a sufficiently low temperature of $T <$ 250 K the initial fast and nearly exponential decay rate is enhanced in the presence of 10 mM KF. In liquid water at room

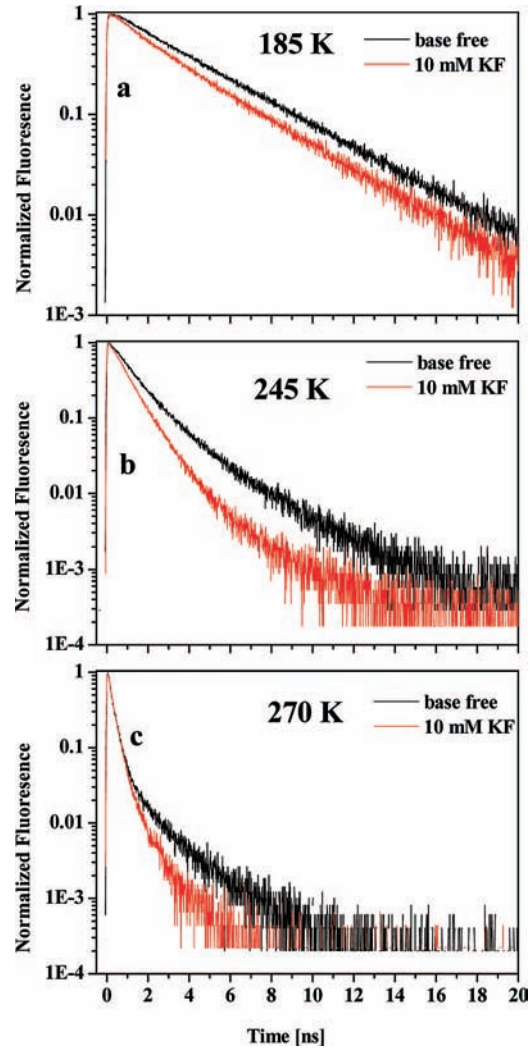

Figure 5. Comparison of the HPTS time-resolved emission of ROH in two samples. The first one contains only HPTS in methanol-doped ice, the second one also contains 10 mM KF.

temperature the proton-transfer rate constant of HPTS is $k_{PT} =$ 10 ns^{-1} thus the proton is transferred with a time constant of about 100 ps. In previous studies[23] we found that the proton-transfer rate constant in ice at ~268 K is smaller by about a factor of 2.5, i.e., $k_{PT} = 4$ ns^{-1}. The temperature dependence of k_{PT} in ice is quite complex. In the high-temperature region of 245 $< T <$ 270 K, the temperature dependence of k_{PT} is large, but not constant. At lower temperatures 220 $< T <$ 245 K, the temperature dependence is rather small, but not constant either. Below 220 K the temperature dependence of k_{PT} of HPTS increases once again. At about 220 K, the value of $k_{PT} \sim 0.2$ ns^{-1} is about the same as the radiative rate constant ($\tau_{rad} \approx 5.3$ ns). The efficiency of the photoprotolytic process strongly reduces at a low temperature when $k_{PT} < k_{rad}$; see eq 1. At $T <$ 220 K in a solution that contains 10 mM KF the rate of proton transfer from HPTS is much larger than in ice samples in the absence of KF.

The most interesting finding in the current study is the efficient proton transfer in the "cold" phase, $T <$ 160 K, in the presence of 10 mM KF. Our cryostat is based on liquid nitrogen as a coolant and this limits the measurements to about 78 K. We found that, in the absence of KF, proton transfer takes place neither in the low-temperature phase in HPTS ($pK^* \approx 1.3$) nor even in the stronger photoacid 2-naphthol-6,8-disulfonate (2N68DS) $pK^* \approx 0.7$. The steady-state emission spectrum of

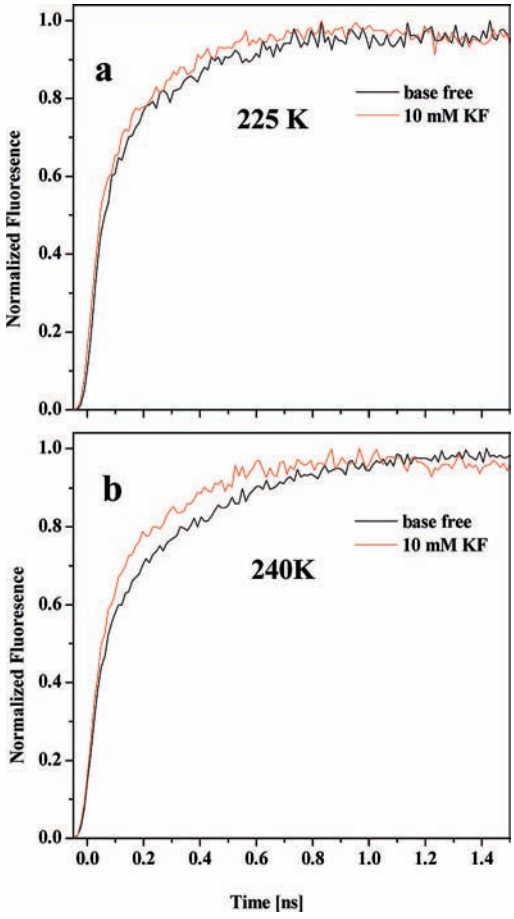

Figure 6. Comparison of the HPTS time-resolved emission of RO^- in two samples. The first one contains HPTS in methanol-doped ice, the second sample also contains 10 mM KF.

HPTS consists of both the protonated ROH form as well as the RO^-; however, the deprotonated form shows large changes in this low-temperature phase. As seen in Figures 1 and 4, both bands shift strongly to the blue and the band width is strongly reduced in this "cold" phase. In a previous paper[24] we found that the solvation dynamics and the solvation energy of 2N68DS and Coumarin 343 in ice show a large change between the high-temperature phase $T > 185$ K and the low-temperature phase $T < 165$ K. Dynamic solvation shift of the excited-state (measured by the time-resolved Stokes shift method) is about 1100 cm^{-1} in the high-temperature region of $T > 200$ K. At a low temperature of $T < 165$ K the solvation energy drops to only about 220 cm^{-1}. In addition to the properties mentioned above we also found that at this low ice temperature a new emission band appears both in Coumarin 343 and in HPTS. In HPTS this emission band is very weak and exhibits a long lifetime of $\tau > 40$ ns. Time-resolved emission measured at $\lambda > 500$ nm shows a long time component of about 1% of the peak intensity of the TCSPC signal at t_+, immediately after the ROH excitation by the laser pulse.

Figure 6 shows the time-resolved emission of the RO^- band at several temperatures measured at about the peak position of the RO^- emission band of two samples. Both samples are slightly acidic and the excitation wavelength is at 400 nm, the peak position of the ROH band. The first ice sample does not contain KF, and the second one contains 10 mM KF. As seen in the figure, at sufficiently low temperatures of $T < 250$ K, the rise-time of the emission curve of samples containing 10 mM KF is faster than that of the samples that do not contain

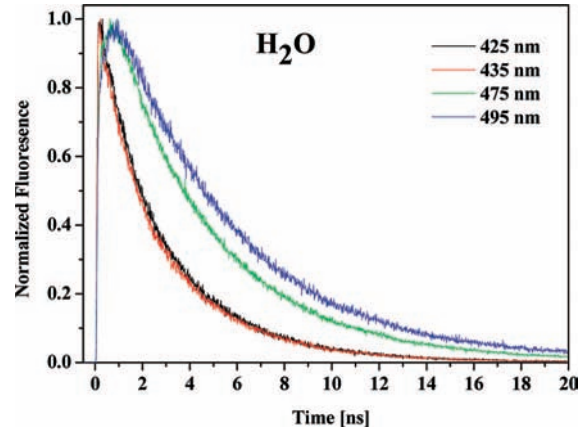

Figure 7. Time-resolved emission of HPTS in H_2O at 145 K measured at four wavelengths: 430, 440, 475 and 495 nm.

KF, indicating that the proton-transfer rate is indeed faster in the case of samples containing KF. We attribute the faster proton-transfer rate to the direct proton-transfer reaction of mobile L-defect created by the F^- with the ROH*.

As mentioned above, in the absence of KF, the ESPT rate is very slow in methanol-doped ice at sufficiently low temperatures, $T < 200$ K, and cannot be detected either by TCSPC signals measured at wavelengths that match the RO^- emission band or by the presence of the RO^- band in the steady-state spectrum. In the presence of 10 mM KF the steady-state spectrum consists of both the ROH and the RO^- emission bands. The RO^- band intensity is comparable to the intensity of the ROH band at the "cold-phase" of $T < 160$ K.

Figure 7 shows the time-resolved emission of HPTS at 148 K measured at four wavelengths: 425, 435, 475 and 495 nm. The ROH emission band of HPTS in the "cold phase" consists of two strong vibronic bands positioned at 425 and 445 nm and successive weaker vibronic bands that also extend their emission to about 520 nm and strongly overlaps with the RO^- emission band. The RO^- emission band in the cold phase also consists of two strong vibronic bands, at about 475 and 495 nm, and the emission extends to about 550 nm.

The time-resolved emission of the ROH band measured at 425 and 435 nm shows a faster decay rate than the radiative rate whereas the signals measured at the RO^- bands positioned at 475 and 495 nm decay with a time constant of 5 ns, the radiative lifetime of both ROH and RO^-. The early time of signals measured at 475 and 495 nm exhibit a rise component with a relative amplitude of about 0.3 and a time constant of a few nanoseconds.

Qualitatively, the decay rate of the ROH signals measured at 425 or 435 nm is comparable to the slow rise-time component of the RO^- signals measured at 475 and 495 nm. The faster decay of the ROH signal and the rise-time component of the RO^- signal are typical for the ESPT process of a photoacid. It is also important to notice that the decay rate at 425 nm is about the same as that at 435 nm, meaning that solvation dynamics is not a major contribution to the signal. In a previous study[24] we noticed that the decay curves of the ROH band of 2N68DS are wavelength dependent. We attributed the fast decay components, found in the time-resolved emission of 2N68DS, to the time dependent red band shift arising from the excited-state solvation process. These components do not contribute to the ROH signals of HPTS in the "cold phase.

Figure 8 shows the time-resolved emission of HPTS in D_2O at 148 K measured at four wavelengths. The signals measured

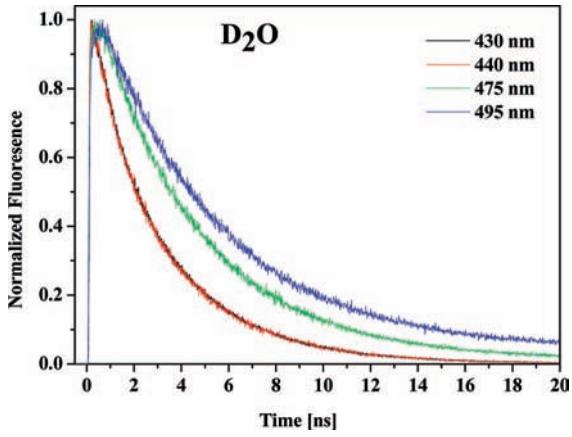

Figure 8. Time-resolved emission of HPTS in D_2O at 145 K measured at four wavelengths: 430, 440, 475 and 495 nm.

at 430 and 440 nm decay faster than the longer wavelength signals. The faster decay is attributed to the direct reaction of the ROH with the L-defect. The rate is somewhat slower than for H_2O samples (as seen in figure 7). The long wavelength time-resolved measurements at 475 and 495 nm clearly show a rise-time component of an amplitude of about 0.3 followed by an exponential decay with a time constant of about 5 ns, which is the radiative decay of the RO^- form.

Discussion

The main findings of this study are as follows:

1. In the ice phase, the L-defect in the ice structure created by the inclusion of fluoride ions reacts with protons that are transferred to ice by a photoacid.

2. In the temperature range $245 > T > 200$ K and in the presence of 10 mM KF, the excited-state proton-transfer rate from HPTS is larger than in the absence of KF. The lower the temperature the larger the ratio $k_{PT}^{KF}(T)/k_{PT}(T)$.

3. Below 240 K (in the absence of KF), the ESPT process from HPTS to methanol-doped ice (1% mole fraction of methanol) is slower than the radiative rate. At about 190 K the ESPT process is inefficient and the deprotonated RO^{-}* form cannot be observed in the steady-state emission spectrum. At temperatures below 160 K the steady-state HPTS emission spectra of ROH (the protonated form) as well as of RO^- (the deprotonated form) show a vibronic structure. At temperatures below 165 K the RO^- band position abruptly shifts to the blue by about 800 cm^{-1}.

4. Below 165 K and in the presence of 10 mM KF, the ESPT from HPTS is efficient unlike the case of HPTS in ice without KF. In the temperature range $165 > T > 78$ K the proton-transfer rate is almost temperature independent.

5. At low temperatures of $T < 165$ K a new, weak emission band of HPTS positioned at a long wavelength of $\lambda > 480$ nm with a long life time of $\tau \approx 40$ ns is observed. The emission gets stronger as the temperature gets lower.

6. The visible light transmittance through an ice sample in the lower temperature region of $T < 160$ K is smaller, by about a factor of 2 than that of an ice sample at $T > 185$ K, indicating that the polycrystallinic ice structure undergoes a change at about 175 K. This finding supports the unusual large change observed in the ESPT process as well as the spectral bandwidth narrowing we find at this low-temperature range in the emission spectra.

In a previous study, we measured the proton transfer in ice and the geminate recombination rates from HPTS and 2N68DS as a function of temperature in the high-temperature region $270 < T < 240$ K.[23] We also studied the ESPT process in liquid water and in ice containing a small amount of a weak base-like acetate or fluoride.[25] We found that both the acetate and fluoride anions can react with a proton that was first transferred to liquid water or ice by an excited photoacid. The proton in ice diffuses and may react with the weak base in the ice. It was found that the proton scavenging effect in ice is much larger than that in the liquid state. We used an explanation for the large scavenging effect, based on the tendency in ice, to concentrate the impurities small and confined volumes in order to minimize the ice crystal energy. The net result of such a process is an effective increase of the base concentration around a photoacid. The larger local concentration increases the proton capture rate. In the current study we further explored the effect of fluoride ion on the proton-transfer rate. We found a profound effect at low temperatures of $78 < T < 240$ K.

Proton Transfer from an Excited Photoacid to Ice in the Presence of a Fluoride Ion. The electrical properties of ice are sensitive to small concentrations of certain impurities that can be incorporated into the hydrogen-bonded network to generate a point defect. HF is the classical example. An HF molecule is substituted for an H_2O molecule in hexagonal ice structure, leaving one bond which lacks a proton. Rotation of H_2O molecule next to it adds a proton to this bond and an L-defect is released into the ice.[4]

L-defects are mobile and react with H_3O^+ and probably with strong and mild acids or acidic sites in ice. The literature value of the mobility activation energy ranges from 0.23 eV[30] to almost zero.[26] The value of the mobility of an L-defect at 218 K is 2.5×10^{-9} m^2 V^{-1} s^{-1} compared to high-temperature proton mobility of 2.8×10^{-8} m^2 V^{-1} s^{-1} at 263 K.[4]

In this study we explain our photoacid photoprotolytic process observations in ice in the presence of KF at sufficiently low temperatures, by proposing the creation of a mobile L-defect in ice by the F^- ions and subsequently a direct reaction with the photoacid itself. There are two L-defect reactions that take place in ice doped with photoacid molecules:

The first L-defect reaction is when the proton is released from the excited photoacid to the ice structure by a laser light pulse. The proton is first transferred to nearby water molecules surrounding the photoacid. The second step is the proton diffusion in the ice crystal. The proton may react with an L-defect created by F^- or recombine geminately with the RO^- form of the photoacid to reproduce the ROH* that may undergo another photocycle.

The second reaction of the L-defect in F^--doped ice is a direct proton transfer from the excited photoacid itself. At sufficiently low temperatures in methanol-doped ice, the conventional proton-transfer rate from an excited-state photoacid to H_2O is much slower than at the highest ice temperature of $T \approx 270$ K. At about 240 K the proton-transfer rate constant from HPTS to ice is about 0.3×10^{-9} s^{-1} compared to about 3.5×10^{-9} s^{-1} at 270 K. At such a low rate constant (time constant of ~3 ns) the L-defect mobility is sufficiently large to enable even the small concentration of L-defect (created by about 10 mM F^- ions) to reach the protonated photoacid within the excited-state lifetime. The proton is being transferred directly from the photoacid to the L-defect. Such a scenario occurs efficiently in 10 mM F^--doped ice at temperatures below $240 > T > 185$ K. Figure 5 shows (at several temperatures) two time-resolved emission transients measured at 440 nm, close to the peak of the ROH emission band of the photoacid. The transient of the F^--doped ice samples decay at a faster rate than the transients in the absence of KF. The faster decay rate in F^--doped samples

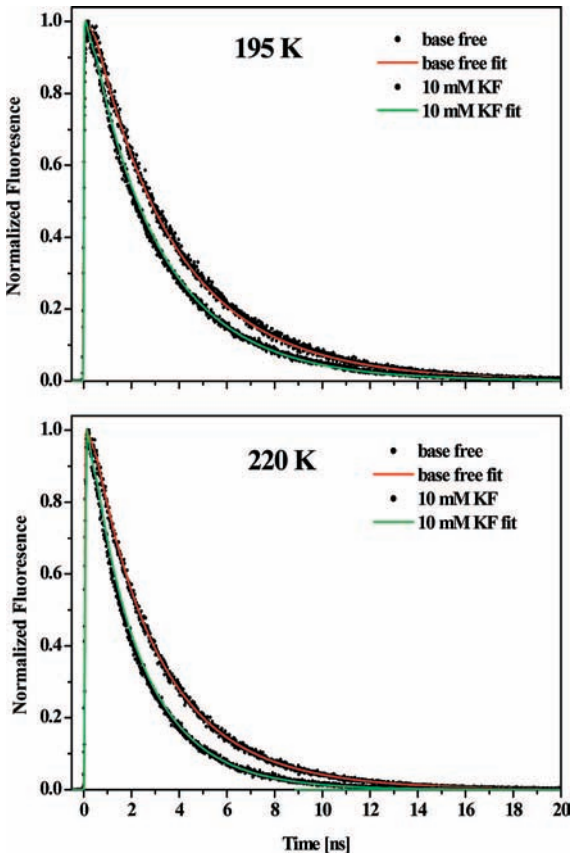

Figure 9. Time-resolved emission of the ROH* band at two temperatures along with computer fits using the diffusion-assisted binary collision model: (symbols) experimental data; (solid line) calculation fits using the model.

starts, at all times, from t_+ (immediately after the pulse excitation) going up to the longest times recorded in the experiments (40 ns). In the past[31] we used a model in liquid solution to describe the direct reaction of a base molecule at a large concentration of $C > 0.5$ M with an excited photoacid molecule. Such a reaction is similar to the one we propose in this study, and which occurs between an excited-state photoacid and an L-defect created by F^- ions incorporated at a lattice site of hexagonal ice. Below, we will briefly describe this model.

The Smoluchowski Model.[32] According to the Smoluchowski model, the survival probability of a single (static) donor (ROH*), due to its irreversible reaction with a concentration $c = [B^-]$ of acceptors, is given by[32–34]

$$S(t) = \exp\left(-c\int_0^t k(t')\,dt'\right) \tag{2}$$

where $k(t)$ is the time-dependent rate coefficient (or, reactive flux at the contact distance, a) for the donor-acceptor pair

$$k(t) = k_{PT}p(a,t) \tag{3}$$

whose proton-transfer rate constant is k_{PT}. The pair (ROH*/B^-) density distribution, $p(r,t)$, is governed by a Smoluchowski equation [diffusion in a potential $U(r)$] in three dimensions[35]

$$\partial p(r,t)/\partial t = Dr^{-2}\frac{\partial}{\partial r}r^2 e^{-\beta U(r)}\frac{\partial}{\partial r}e^{\beta U(r)}p(r,t) \tag{4}$$

where D is the relative diffusion coefficient of the pair, $U(r)$ their interaction potential, $\beta = 1/k_BT$ and k_BT is the thermal energy. To calculate $k(t)$, one imposes an initial equilibrium distribution

$$p(r,0) = \exp[-\beta U(r)] \tag{5}$$

and a "radiation" boundary condition at the contact distance ($r = a$), depicting irreversible recombination occurring upon binary collision.[23]

The interaction potential, $U(r)$, was taken as the Debye−Hückel (DH) screened Coulomb potential.[36]

We solved eq 4 numerically, using a user-friendly Windows application for Spherically-Symmetric Diffusion Problems (SSDP, ver. 2.61)[37] to yield $k(t)$ of eq 3.

When a potential is introduced, it behaves correctly at both $t = 0$ and $t = \infty$ and the values of $k(t)$ at $t = 0$ and $t = \infty$ are given by

$$k(0) = k_{PT}e^{-\beta U(a)} \qquad k(\infty) = [k(0)^{-1} + k_{D^{-1}}]^{-1} \tag{6}$$

where $k_D = 4\pi D a_e$ is the diffusion-control rate constant and a_e is an effective contact radius. The non-exponentiality in $S(t)$ is a result of a time-dependent rate constant $k(t)$, as depicted by the ratio $k(0)/k(\infty)$.

From the time dependent rate constant, $k(t)$, one can calculate the survival probability of an ROH* molecule surrounded by an equilibrium distribution of ions, according to eq 2. To account the for conventional ESPT process and the pure radiative lifetime of ROH, which occurs in parallel and supposedly independently from the reaction in eq 1, we write

$$S'(t) = \exp(-t/\tau - c\int_0^t k(t')\,dt') \tag{7}$$

where $1/\tau = \tau_{rad} + 1/\tau_{PT}$. This quantity, with an independently measured τ (in the absence of KF) , is used in comparison with the experimental signal.

Model Fitting of the Experimental Results. Figure 9 shows the model fitting of the time-resolved emission of the ROH form of HPTS in methanol-doped ice in the presence of 10 mM KF at two temperatures. We used the model described above to account for the reaction

$$L + ROH^* \rightarrow LH^+ + RO^-* \tag{8}$$

The ROH* proton is transferred directly to a mobile L-defect. This reaction depends on several parameters. The parameters used in our model are the concentration of L-defect c_L, the diffusion constant of the L-defect D_L, the intrinsic reaction rate constant k_{PT}^L, and the contact radius of the reaction a_L. In addition to the parameters mentioned above, we have to take into account the Debye−Hückel screening of the Coulomb potential due to the presence of KF in ice and the effective charge of an L-defect -0.38 e, where e is the electronic charge.

We got a good fit to the experimental results using the following parameters. At the contact sphere, the reaction rate constant k_{PT}^L,was about 100 ns^{-1}. In our previous studies we got such a large rate constant in liquid water using a large concentration of acetate base ($c > 0.5$ M) which reacts directly with HPTS ROH ($k = 150$ ns^{-1}). Mohammed et al.[38] found a similar rate constant for the reaction between excited HPTS and concentrated solutions of acetate, $c > 1$ M that form a "loose complex" already in the ground state. At 220 K the value of the diffusion constant of the L-defects is 2.5×10^{-6} cm^2/s. This value is close to the value calculated from the Einstein−Stokes relation, which was the published mobility value of 2.5×10^{-9} m^2/V at 218 K. For a good fit we had to compromise on the value of the L-defect local concentration c_L. The effective L-defect concentration we used in the fit is 50 mM, and the KF concentration is only 10 mM. The concentration enters the calculations in eq 7, and it basically affects the diffusion step. The larger the concentration the smaller the number of steps the random walker needs to reach the reaction sphere. The larger

effective concentration of L-defect may indicate that the L-defect motion not only is a pure random walk of short distance steps but also exhibits some longer jumps. According to molecular dynamic simulations[9] the defect motion cannot be described as random diffusion between all available sites; rather, preferred paths are present. A defect seems to drift through ice, while getting trapped at some preferential sites and performing excursions around these sites. The time spent at the "trap sites" is typically several picoseconds but may be as long as a few tens of picoseconds.[9] We also found that it is necessary to use a rather large contact radius $a = 10$ Å to obtain a good fit at all times. In previous studies[31] we used $a = 7$ Å in the liquid state, Weller[12] used that value for the contact radius of the acetate reaction with a photoacid. The larger value for the contact sphere radius supports the results of Buch's[9] simulation of L-defect motion in a preferred ice path. It can also fit the picture that the proton-transfer reaction does not occur at a contact point between the L-defect and the hydroxyl group of HPTS, but rather the proton jumps a longer distance to the L-defect. The proton jumps to the L-defect via a bridge of one or two water molecules. This picture has some similarity with the "loose complex" proton-transfer mechanism of Mohammed et al.[38] In their model the photoacid and the proton acceptor (acetate) are separated by a water molecule. Recently the separation of HPTS from acetate by a water molecule has been shown to slow the ESPT process in a cyclodextrin inclusion complex.[39]

L-Defect Diffusion Dependence on the Methanol Concentration. Pure ice is known to be a bad solvent.[4] It occurs that upon controlled slow freezing most of the dopants are extracted out of the crystal and therefore concentrate at the grain boundary. In our initial experiments on the photoprotolytic cycle of the photoacid in pure ice,[21,22] we noticed that the frozen samples are non-fluorescent, whereas for the liquid samples the fluorescence is at least 3 orders of magnitude more intense. We found a procedure to overcome the aggregation of the photoacid molecules upon sample freezing. To prevent the aggregation, we added to a pure aqueous solution 1% of methanol (by mole ratio). The methanol probably serves as a mediator between the hydrophobic aromatic rings of the photoacid with the ice water molecules. In numerous experiments we found that the fluorescence intensity of the frozen methanol-doped ice sample containing the photoacid is "behaving properly".

In this study we found that the L-defect diffusion constant of ice strongly depends on the methanol concentration. The L-defect diffusion constant decreases as the methanol concentration increases. We explain this effect by the ability of methanol to capture the L-defect with a fast rate and to release it at a much slower rate. Thus, the methanol serves as an L-defect trap within the experimental time window. The overall effect is a reduction in the effective diffusion constant within the methanol-doped ice crystal. The question that then arises is why to dope ice with methanol? The methanol doping is necessary to incorporate the photoacid in the crystal bulk, and prevent the exclusion of the photoacid from the bulk and its aggregation at the grain boundaries.

Proton-Transfer Process in the "Cold Phase". As mentioned above, the temperature dependence of the ESPT process in methanol-doped ice at $270 > T > 190$ K shows three distinct ranges.[23] Below about 190 K, HPTS is incapable of transferring a proton to ice within the excited-state lifetime, where the radiative lifetime is about 5 ns. In addition to the ESPT process, we found from the solvation dynamics experiments that at $T <$ 165 K the dynamic solvation shift drastically reduces from about 1100 cm^{-1} at $T > 220$ K to about 200 cm^{-1} at $T \approx 160$ K. In addition, the emission spectrum of the RO^- at low temperature shows a phase transition behavior (see Figure 1). The emission spectrum of RO^- in the high-temperature range is structureless with a peak position at about 500 nm at 200 K. The RO^- spectrum in the low-temperature range exhibits a rather distinctive vibronic structure with the high-energy peak position at a wavelength of about 475 nm that shifted by about 800 cm^{-1} to the blue with respect to the high-temperature spectrum. On the basis of the distinctive spectroscopic properties of the low-temperature methanol-doped ice at $T < 170$ K, we will refer to the ice structure as the "cold-phase". Thus far we do not have X-ray data or similar information to confirm a new ice phase at $T < 170$ K. In the literature there are large numbers of studies reporting on the properties and structures of a meta-stable low-temperature phase designated "ice I_c" in which the oxygens are arranged in a cubic diamond structure rather than on the hexagonal lattice of the regular I_h.[40] From a large number of experiments[40] it is clear that ice I_c is always meta-stable and the temperature at which it transforms to ice I_h is determined by the process of molecular rearrangement. As published in the literature, the temperature of the phase transition between I_c and I_h ranges from 130 K up to 200 K.

In the "cold phase" in the presence of 10 mM KF we observed the following unique properties:

1. The HPTS ROH and RO^- emission spectra are vibronically structured because the individual width of each vibronic band is much smaller than at the high-temperature phase (I_h). In the cold phase the RO^- band maximum exhibits a marked blue shift by 800 cm^{-1}.

2. In the absence of KF the ESPT process is not operative and the emission spectrum of a sample that is excited from the ground state of the ROH form consists of only the band of the ROH.

3. The dynamical part of the solvation energy reduced in the cold phase to about 200 cm^{-1} compared to about 1100 cm^{-1} in the high-temperature phase.[24]

4. Excited-state proton transfer takes place from HPTS in the presence of 10 mM KF. The activation energy of the ESPT process between 160 K down to 78 K is very small.

5. The ESPT rate in the "cold phase" is larger by about a factor of 2 than in high-temperature ice at 190 K.

6. The kinetic isotope effect (KIE) k_{PT}^H/k_{PT}^D is very small in the "cold phase", whereas in the high-temperature phase the KIE is much larger. In the temperature range of $270 > T > 240$ K the KIE is approximately constant, i.e, KIE $\cong 3$.

We explain the low-temperature "cold phase" ESPT data by the following process. The regular excited-state proton-transfer mechanism is not operative in the "cold phase" and thus, in the absence of KF, no proton-transfer process takes place. Introducing fluoride ions into the ice structure creates mobile L-defects. In general, the mobile L-defect reacts with H_3O^+ and other acid or acidic sites in the ice. The concentration of L-defect in pure ice at 270 K is estimated to be very small, 10^{-7}.[4] At low temperatures it is even smaller because of a relatively large activation energy associated with a D−L pair formation, which is in the range 0.66–0.79 eV.[41] The mobility of the L-defect in high-temperature ice is large, comparable to that of the H_3O^+ ionic defect. The activation energy of the mobility of L-defect is small (less than 0.23 eV).[26] In 10 mM KF-doped ice the concentration of L-defect is comparable to a KF concentration and is thus larger than undoped ice by many orders of magnitude. The main purpose of the lengthy description of the L-defect properties is to propose that in the "cold phase" the mechanism of excited-state proton transfer occurs by a direct

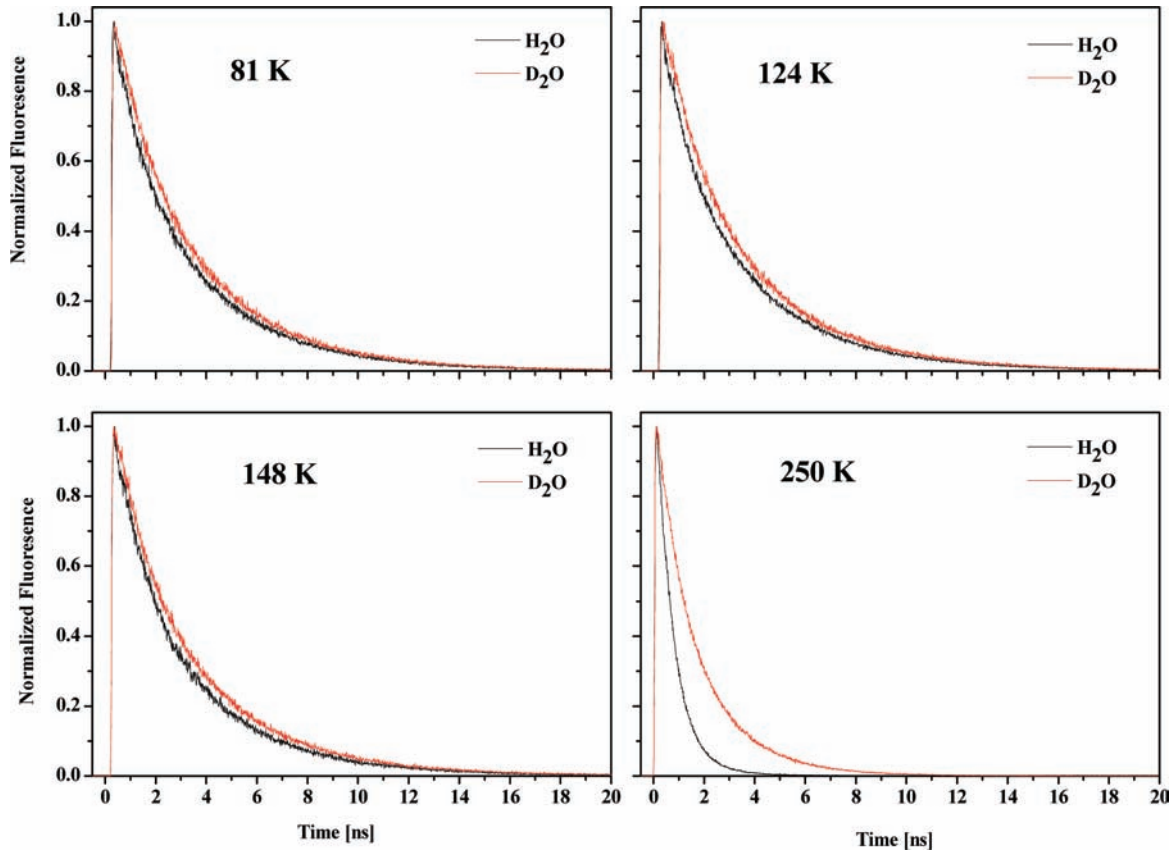

Figure 10. Time-resolved emission of the ROH* of HPTS at several low temperatures in H_2O and D_2O samples. Note the small isotope effect at temperatures below 150 K.

proton transfer from an excited photoacid molecule to L-defect. First the L-defect moves toward the excited molecule with the transfer of a proton only taking place at a contact sphere next to the photoacid. The reaction can be described by the Smoluchowski theory of diffusion-assisted binary collision. We explained the experimental results, marked in the "properties list" above as 4–6, as arising from the unique properties of the L-defect and the binary collision mechanism. In point 4 we stated that the activation energy of the ESPT process is small. This can be explained by the low activation energy of the mobility of L-defects in general and in the "cold phase" in particular.

In point 5 we compared the proton-transfer rate in the high-temperature phase to the rate in the "cold phase. Despite the usual decrease of the rate of dynamical processes with the temperature decrease, in the "cold phase" the ESPT rate is larger by about a factor of two than in the high-temperature phase. We explained this faster rate by the L-defect "cold phase" properties. If the "cold phase" is the "I_c" phase, then the increase of the ESPT rate in the "cold phase" is attributed to the larger L-defect mobility in the "I_c" phase. We are unaware of published values of L-defect motilities in the "I_c" phase.

Point 6 concerns the small kinetic isotope effect in the "cold phase. Figure 10 shows the time-resolved emission of the ROH form of HPTS measured at 440 nm for H_2O and D_2O samples at several temperatures. As seen in the figure, at temperatures below 150 K the D_2O decay time is slightly slower than that of the H_2O sample. For comparison we also plot the ROH decay for H_2O and D_2O at 250 K to show that the ESPT kinetic isotope effect at this high temperature is much larger. The isotope effect of the intrinsic ESPT rate constant k_{PT} is large in both ice and water KIE, i.e., $\approx$3. In the liquid phase the KIE on proton mobility is rather small being $\mu_H{}^+\backslash\mu_D{}^+ \cong 1.4$. In high-temperature ice we found that the KIE of proton/deuteron mobility is of the same order as well.[42] From eq 6 the long time rate constant $k(\infty)$ depends on both k_{PT} and k_D. The time-resolved emission in the "cold phase" is mostly dominated by k_D, the diffusion rate constant, and not by the intrinsic rate, thus explaining the small observed isotope effect in the ESPT due to the small KIE in the L-defect mobility in the cold phase. As mentioned before according to molecular dynamic simulations[9] the defect moves along preferred paths. A defect seems to drift through ice, while getting trapped at some preferential sites.

Alternative Explanation to the Effect of KF in Ice. An alternative explanation to the strikingly large L-defect effect on the time-resolved emission of HPTS in ice is along the line of many other observations[43–46] that dopants tend to exclude from the ice bulk and tends to aggregate on grain boundaries. In such a case the photoacid molecules in our experiments are not incorporated in the bulk of a microcrystal of ice rather than the photoacids position is at the grain boundaries. The L-defect reaction with the ROH is taking place at the grain boundaries, rather than in the bulk.

Devlin and coworkers studied[45,46] ice samples prepared by careful and controlled deposition of water molecules on cold surfaces by spraying water and dopants. In many studies they found that the dopants tend to diffuse toward the sample surface. Molecular dynamics simulations by Devlin et al.[46] confirm the experimental observation of the tendency of dopants to extract from the bulk and positioned at the surface. Devlin found that protons stay in the bulk, and the counter ion, the chloride in the case of HCl, tends to move to the surface area. Let us assume that the photoacids themselves are at the grain boundaries as well as the counter ions (sodium ions from the sulfonates of

HPTS as well as the fluoride and potassium ions from KF). The L-defect position is in the bulk of the microcrystals. In such a case the photoacid concentration is very large at the surface, whereas the L-defect concentration at the grain boundaries is small and probably equal to that of the bulk. The photoprotolytic cycle takes place at the surface of the polycrystalline ice. The F^- ion is immobile at the frozen grain boundaries. The experimental results then are indicative of a very large L-defect diffusion constant at the grain boundaries.

Summary

We used steady-state and time-resolved emission techniques to study the photoprotolytic cycle of an excited photoacid in methanol-doped ice in the presence of a low concentration of a weak base-like F^-. Below 240 K (in the absence of KF) the ESPT process from HPTS to methanol-doped ice (1% mole fraction of methanol) was slower than the radiative rate. At about 190 K and temperatures below the ESPT process is inefficient. At temperatures below 160 K the steady-state emission spectra of both the ROH (the protonated form) and the RO^- (the deprotonated) form of HPTS showed a vibronic structure. At temperatures below 160 K the RO^- band position abruptly shifts to the blue by about 800 cm^{-1}. We referred to the large change in the spectroscopic properties of the HPTS emission bands as indicating a phase transition.

Unlike the case of HPTS in ice without KF, below 165 K and in the presence of 10 mM KF, the ESPT from HPTS is efficient. In the temperature range of 165 K > T > 78 K the proton-transfer rate is almost temperature independent. We explained the low-temperature "cold phase" ESPT data by the following process. The regular excited-state proton-transfer mechanism is not operative in the "cold phase" and thus, in the absence of KF, no proton-transfer process takes place. Introducing fluoride ions into the ice structure creates mobile L-defects. The mechanism of excited-state proton transfer in the "cold phase" is by direct proton transfer from an excited photoacid molecule to L-defect. First the L-defect moves toward the excited molecule with the transfer of a proton only taking place at a contact sphere next to the photoacid. The reaction can be described by the Smoluchowski theory of a diffusion-assisted binary collision. The time-resolved emission in the "cold phase" is mostly dominated by k_D, the diffusion rate constant, and not by the intrinsic rate, which is very fast. The small observed isotope effect in the ESPT is due to the small KIE in the L-defect mobility in the "cold phase".

Acknowledgment. We thank Prof. V. Buch and Dr. H. Diamant for their helpful and fruitful suggestions and discussions. This work was supported by grants from the Binational US-Israel Science Foundation and the James-Franck German-Israel Program in Laser-Matter Interaction.

References and Notes

(1) Fletcher N. H. *The Chemical Physics and of Ice*; Cambridge University Press: Cambridge, U.K., 1970; Chapter 9.
(2) Hobbs, P. V. *Ice Physics*; Clarendon Press: Oxford, U.K., 1974; Chapter 2.
(3) Von Hippel, A.; Runck, A. H.; Westphal, W. B. In *Physics and Chemistry of Ice*; Walley, E., Jones, S. J., Gold, L. W., Eds.; Royal Society of Canada: Ottawa, 1973.
(4) Petrenko, V. F.; Whitworth, R. W. *The physics of ice*; Oxford University: Oxford, U.K., 1999.
(5) Kelly, I. J.; Salomon, R. R. *J. Phys. Chem.* **1969**, *50*, 75.
(6) Jaccard, C. *Ann. N. Y. Acad. Sci.* **1965**, *125*, 390.
(7) Bjerrum, N. *Science* **1952**, *115*, 385.
(8) Kobayashi, C.; Saito, S.; Ohmine, I. *J. Chem. Phys.* **2001**, *115*, 4742.
(9) Podeszwa, R.; Buch, V. *Phys. Rev. Lett.* **1999**, *83*, 4570.
(10) Bell, R. P. *The Proton in Chemistry*, 2nd ed; Chapman and Hall: London, 1973.
(11) *Proton Transfer Reaction*; Caldin, E. F., Gold, V., Eds.; Chapman and Hall: London, 1975.
(12) (a) Weller, A. *Prog. React. Kinet.* **1961**, *1*, 189. (b) *Z. Phys Chem. N. F.* 1958, *17*, 224.
(13) Ireland, J. E.; Wyatt, P. A. *Adv. Phys. Org. Chem.* **1976**, *12*, 131.
(14) (a) Gutman, M.; Nachliel, E. *Biochim. Biophys. Acta* **1990**, *391*, 1015. (b) Pines, E.; Huppert, D. *J. Phys. Chem.* **1983**, *87*, 4471.
(15) Kosower, E. M.; Huppert, D. *Annu. Rev. Phys. Chem.* **1986**, *37*, 127.
(16) Tolbert, L. M.; Solntsev, K. M. *Acc. Chem. Res.* **2002**, *35*, 1.
(17) Rini, M.; Magnes, B. Z.; Pines, E.; Nibbering, T. J. *Science* **2003**, *301*, 349.
(18) Prayer, C.; Gustavsson, T.; Tarn-Thi, T. H. *Fast Elementary Processes in Chemical and Biological Systems 54th International Meeting of Physical Chemistry*; American Institute of Publishers: New York, 1996; p 333.
(19) Tran-Thi, T. H.; Gustavsson, T.; Prayer, C.; Pommeret, S.; Hynes, J. T. *Chem. Phys. Lett.* **2000**, *329*, 421.
(20) Agmon, N. *J. Phys. Chem. A* **2005**, *109*, 13.
(21) Leiderman, P.; Gepshtein, R.; Uritski, A.; Genosar, L.; Huppert, D. *J. Phys. Chem. A* **2006**, *110*, 9039.
(22) Uritski, A.; Leiderman, P.; Huppert, D. *J. Phys. Chem A* **2006**, *110*, 13686.
(23) Leiderman, P.; Uritski, A.; Huppert, D. *J. Phys. Chem. A* **2007**, *111*, 4998.
(24) Uritski, A.; Huppert, D. *J. Phys. Chem A* **2007**, *111*, 10544.
(25) Uritski, A.; Leiderman, P.; Huppert, D. *J. Phys. Chem C* **2007**, *111*, 8856.
(26) Kunst, M.; Warman, J. M. *J. Phys. Chem.* **1983**, *87*, 4093.
(27) Pines, E.; Huppert, D.; Agmon, N. *J. Chem. Phys.* **1988**, *88*, 5620.
(28) Uritski, A.; Huppert, D. *J. Phys. Chem. A* **2008**, in press.
(29) Fraser, R. D. B.; Suzuki, E. In *Spectral Analysis*; Blackburn, J. A., Ed.; Marcel Dekker: New York, 1970; p 171.
(30) Jaccard, C. *Helv. Phys. Acta* **1959**, *32*, 89.
(31) Cohen, B.; Huppert, D.; Agmon, N. *J. Phys. Chem. A* **2001**, *105*, 7165.
(32) Von Smoluchowski, M. *Z. Phys. Chem.* **1917**, *92*, 129.
(33) Tachiya, M. *Radiat. Phys. Chem.* **1983**, *21*, 167.
(34) Szabo, A. *J. Phys. Chem.* **1989**, *93*, 6929.
(35) Rice, S. A. In *Comprehensie Chemical Kinetics*; Bamford, C. H., Tipper, C. F. H., Compton, R. G., Eds.; Elsevier: Amsterdam, 1985; Vol. 25.
(36) Robinson, R. A.; Stokes, R. H. *Electrolyte Solutions*, 2nd ed.; Butterworths: London, 1959.
(37) Krissinel′, E. B.; Agmon, N. *J. Comput. Chem.* **1996**, *17*, 1085.
(38) Mohammed, O. F.; Pines, D.; Dreyer, J.; Pines, E.; Nibbering, E. T. J. *Science* **2005**, *310*, 5745.
(39) Sahu, S. K. M. K.; Ghosh, S.; Sen, P.; Bhattacharyya, K. *J. Phys. Chem. A* **2006**, *110*, 13646.
(40) Petrenko, V. F.; Whitworth, R. W. *The physics of ice*; Oxford University: Oxford, U.K., 1999; Chapter 11.8.
(41) Petrenko, V. F.; Whitworth, R. W. *The physics of ice*; Oxford University: Oxford, U.K., 1999; Table 4.6.
(42) Poles, E.; Cohen, B.; Huppert, D. *Isr. J. Chem.* **1991**, *39*, 347.
(43) Heger, D.; Klànovà, J.; Klàn, P. *J. Phys. Chem. B* **2006**, *110*, 1277.
(44) Takenaka, N.; Tanaka, M.; Okitsu, K.; Bandow, H. *J. Phys. Chem. A* **2006**, *110*, 10628.
(45) Devlin, J. P.; Gulluru, D. B.; Buch, V. *J. Phys. Chem. B* **2005**, *109*, 3392.
(46) Devlin, J. P.; Uras, N.; Sadlej, J.; Buch, V. *Nature* **2002**, *417*, 269.

JP711030M